Limitations on Vibration Isolation for Microgravity Space Experiments

C. Knospe* and P. Allaire†
University of Virginia, Charlottesville, Virginia 22901

The limitations on vibration isolation for microgravity space experiments are explored. These limitations result from the restricted interior space available for vibration isolation and the strokes required to achieve isolation. A one-degree-of-freedom representation of the experiment spacecraft system is used, and an ideal vibration actuator is assumed. The wall motion is characterized as sinusoidal at a single frequency. A kinematic representation results, and the problem becomes one of finding the minimum acceleration trajectory within a pair of moving walls. This optimal control problem can be solved via the calculus of variations; however, transcendental equations result. To obtain an analytic solution, the inequality constraints are dropped and initial and final conditions on the trajectory are added. The resulting control is optimal if the inequality constraints are still satisfied. Analysis yields a simple condition under which a closed-form solution is available. A suboptimal solution that always satisfies the inequality constraints is also presented. This solution is shown to have performance very close to optimal. The minimum experiment rms acceleration given the spacecraft vibration frequency and amplitude is obtained from the optimal and suboptimal solutions. Plots are presented, and the limitations on vibration isolation are discussed. These results demonstrate that isolation from low-frequency vibration requires more interior space than is available for vibration isolation on manned space orbiters.

Nomenclature

A = matrix in state dynamics
B = vector in state dynamics
A = amplitude of base motion
c_i = coefficients of optimal control u_{opt}
F_u = force on experiment platform
H = Hamiltonian
J = cost function
m = experiment mass
L = stroke (maximum translation of experiment)
T = half-period
t = time
t^* = boundary constraint exit time
u = control acceleration
x = state vector, $=(x_1, x_2)^T$
x, x_1 = position of experiment platform
x_2 = velocity of experiment platform
y = position of base
f = frequency of base motion, Hz
α = coefficient of optimal control u_{opt_2}
λ = Lagrange multiplier
ω = frequency of base motion

I. Introduction

THE use of a microgravity environment in space has the potential for advanced materials science experiments. Spencer[1] outlined the goals as 1) an understanding of basic physical phenomena, 2) quantification of limitations and effects imposed by gravity, and 3) application of knowledge to Earth- and space-based processes or products. A microgravity environment can potentially eliminate buoyancy-driven convection, sedimentation, and hydrostatic pressure, and it can have several other advantages.[1]

At this point in time, the actual acceleration requirements for various experiments are not well known.[2] An assessment of existing theoretical and experimental data available up to 1985 was carried out in Ref. 3. Results indicate that acceleration levels below $10^{-6} g_0$ at frequencies below 0.1 Hz are required by many processes, but the requirements are somewhat relaxed at higher frequencies. Work to better determine the levels needed is in progress. An example is a twin-crystal growth experiment to be carried out on spacecraft.[4]

An essential part of the development of a microgravity experiment program is the characterization of the low-acceleration environment aboard manned space orbiters. NASA has carried out a series of measurements reported at various conferences.[5,6] A summary of these data was presented by Grodsinsky and Brown[7] and is repeated in Table 1. Additional data on the Space Transportation System was presented in Ref. 8. Similar results have been reported by the European Space Agency.[9]

Vibration levels reported in the aforementioned literature for spacecraft are significantly higher than allowable for materials science experiments. In order to achieve accurate and reproducible results in such experiments, vibration isolation will be required.[3] Acceleration disturbances in the orbiter environment cover a wide frequency bandwidth, from dc to 100 Hz. Sources below 10^{-3} Hz include drag, light pressure oscillations, tidal effects, and gravity gradients. Above this frequency, sources include manned activity, thruster firing, and orbiter flight systems. The frequencies and amplitudes of these accelerations are summarized in Table 1. Low-frequency (10^{-3} to 10^{-2} Hz) structural excitations likely to be present on the space station are not represented in this data. Such flexible structure modes will contribute significantly to the vibration environment.

The capability of isolating the experiment from any particular vibration source is dependent on both frequency and amplitude. At relatively high frequencies, above about 5 Hz, passive vibration isolation is normally possible. Examples include the Hubble space telescope reaction wheel isolation system[10] and viscous dampers for reduced jitter.[11] One of the few active vibration isolation systems is reported in Ref. 12. The volume available in spacecraft for experiments is limited. Therefore, this introduces an additional constraint on active isolation systems.

Received Dec. 21, 1989; revision received March 21, 1990.

*Research Assistant Professor, Department of Mechanical and Aerospace Engineering.
†Professor, Department of Mechanical and Aerospace Engineering.

Table 1 Microgravity space experiment acceleration environment (from Ref. 7)

g/g_0	F, Hz	Source
Quasisteady or dc acceleration disturbances		
10^{-7}	$0-10^{-3}$	Aerodynamic drag
10^{-8}	$0-10^{-3}$	Light pressure
10^{-7}	$0-10^{-3}$	Gravity gradient
Periodic acceleration disturbances		
2×10^{-2}	9	Thruster fire (orbital)
2×10^{-3}	5–20	Crew motion
2×10^{-4}	17	Ku-band antenna
Nonperiodic acceleration disturbances		
10^{-4}	1	Thruster fire (attitude)
10^{-4}	1	Crew pushoff

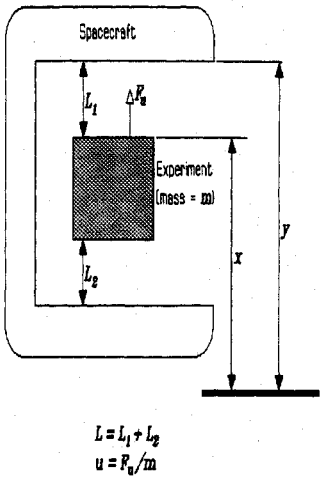

Fig. 1 Kinematic representation of the experiment spacecraft system.

The purpose of this paper is to explore the limitations on vibration isolation for space experiments, rather than to develop the actual control algorithm. Thus, the ideal vibration actuator is assumed, and an optimal control is formulated. The optimal control problem is solved for a sinusoidal excitation to obtain the minimum acceleration trajectory. A suboptimal solution that gives results close to optimal is also explored.

II. Kinematic Formulation

For this analysis, a one-dimensional theory is developed. Clearly, the actual system required will be multidimensional so this work is preliminary in nature. Consider a one-degree-of-freedom system, the experiment, as illustrated in Fig. 1 with position $x(t)$. It is connected to the spacecraft by umbilicals, such as power or fluid lines, and by a vibration isolation actuator. A similar geometry is discussed by Genkin et al.,[13] with stiffness and damping as well as an active vibration isolation actuator. However, that system has one side fixed to the ground and the forced mass in motion. Although the spacecraft actually has a finite mass, it may be considered to have infinite impedance for this analysis since the spacecraft-to-experiment weight ratio is very large. Thus, the spacecraft acts as an external base motion $y(t)$ transmitting forces through the umbilicals and the actuator.

This representation reduces the problem to a kinematic one. Onboard the spacecraft, available interior space for the experiment is limited. The walls around the experiment, which should not be contacted, constrain the maximum translation of the experiment, or stroke, to a fixed distance L. The base motion $y(t)$ imposed on the walls, spaced to permit a stroke of L, forms the problem constraints. The problem of vibration isolation/attenuation becomes one of finding the optimal trajectory (minimum acceleration) given the constraint conditions (moving walls).

III. Optimal Control Formulation

The objective is to formulate and solve the optimal control problem for minimum experiment acceleration trajectory in time. Let the experiment acceleration be denoted as u ($u = F_u/m$). Then the cost function J to be minimized is

$$J = \int_0^\infty u^2 \, dt \tag{1}$$

with the constraint

$$y(t) - L \le x(t) \le y(t), \qquad 0 \le t \tag{2}$$

for a given base motion $y(t)$.

This problem is examined for harmonic base motion at a single frequency. Let $y(t)$ have the form

$$y(t) = A[1 - \cos(\omega t)] \tag{3}$$

with the half-period $T = \pi/\omega$. The cost function J now simplifies to

$$J = \int_0^T u^2 \, dt \tag{4}$$

due to the periodicity of the problem. Also, the constraint becomes

$$A[1-\cos(\pi t/T)] - L \le x(t) \le A[1-\cos(\pi t/T)] \qquad 0 \le t \le T \tag{5}$$

over the half-period.

This problem may be viewed as finding the optimal path through sinusoidally oscillating walls, as illustrated in Fig. 2. If the base travel $2A$ is smaller than the space L, the minimum acceleration is zero and the problem trivial. However, if the base travel $2A$ is larger than the space available for vibration isolation L, then the optimization problem has active inequality constraints on the state variables. The solution to this problem may be attempted using the calculus-of-variations approach by adjoining the Hamiltonian with a second-order state-variable inequality constraint. This method requires the satisfaction of two interior boundary conditions (position and velocity continuity) at the junction points of constrained and unconstrained path arcs.[14] Because the wall motion is sinusoidal, these tangency constraints require the solution of several transcendental equations. Therefore, no closed-form solution to the general problem is available. As will be shown, under a certain condition the problem can be solved to yield an analytic solution. When this condition does not hold, a suboptimal solution may be employed. Thus, easy-to-use equations and plots for determining vibration isolation limits are made available to microgravity experiment designers.

IV. Analytic Solution

To obtain an analytic solution to the problem, the constraints are simplified to the boundary conditions

$$x(0) = 0, \qquad x(T) = 2A - L \ge 0$$
$$\dot{x}(0) = 0, \qquad \dot{x}(T) = 0 \tag{6}$$

which an optimal solution clearly must satisfy.

Define the system state variables[15] as

$$x_1 = x, \qquad \dot{x}_1 = x_2, \qquad \dot{x}_2 = u \tag{7}$$

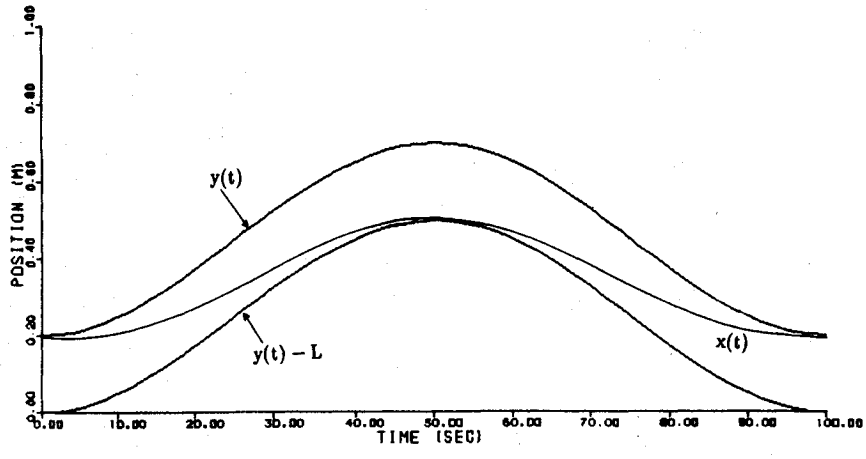

Fig. 2 Optimal path through harmonic walls.

and the equations of motion become

$$\dot{\boldsymbol{x}} = \boldsymbol{A}\boldsymbol{x} + \boldsymbol{B}u$$

$$\boldsymbol{x}^T = [x_1 \quad x_2], \qquad \boldsymbol{A} = \begin{bmatrix} 0 & 1 \\ 0 & 0 \end{bmatrix}, \qquad \boldsymbol{B}^T = [0 \quad 1] \tag{8}$$

The cost function is adjoined by the constraint, Eq. (7), using two Lagrange multipliers.[16] The result is

$$J = \int_0^T [u^2 + \lambda_1(x_2 - \dot{x}_1) + \lambda_2(u - \dot{x}_2)]\, dt \tag{9}$$

which is the general functional for this problem.

Define the Hamiltonian as

$$H = u^2 + \lambda_1 x_2 + \lambda_2 u \tag{10}$$

If we employ the calculus of variations, the minimization equations are

$$\dot{\lambda}_1 \equiv -\frac{\partial H}{\partial x_1} = 0$$

$$\dot{\lambda}_2 \equiv -\frac{\partial H}{\partial x_2} = -\lambda_1$$

$$0 \equiv \frac{\partial H}{\partial u} = 2u + \lambda_2 \tag{11}$$

Solving these gives

$$\lambda_1 = c_0$$

$$\lambda_2 = -c_0 t + c_1$$

$$u = \tfrac{1}{2}c_0 t - \tfrac{1}{2}c_1 \tag{12}$$

Imposing the boundary conditions of Eq. (6) yields

$$c_0 = -24(2A - L)/T^3$$

$$c_1 = -12(2A - L)/T^2 \tag{13}$$

and

$$u(t)_{\text{opt}} = \frac{-12(2A - L)}{T^3} t + \frac{6(2A - L)}{T^2}$$

$$\dot{x}(t) = \frac{-6(2A - L)}{T^3} t^2 + \frac{6(2A - L)}{T^2} t$$

$$x(t) = \frac{-2(2A - L)}{T^3} t^3 + \frac{3(2A - L)}{T^2} t^2 \tag{14}$$

$$2A - L \geq 0$$

(Of course, if $2A - L < 0$, the optimal trajectory is clearly $u = 0$, $\dot{x} = 0$, $x = 0$.) The root-mean-square (rms) acceleration of this trajectory is

$$\text{rms}(\ddot{x}_{\text{opt}}) = \left(\frac{1}{T}\int_0^T u^2\, dt\right)^{1/2} = \frac{\sqrt{12}(2A - L)}{T^2} \tag{15}$$

The trajectory of Eq. (10) is the solution to the original problem if the inequality constraints on the platform position, Eq. (5), are satisfied. Note that Eq. (14) is a linear open-loop control law.

V. Conditions on the Analytic Solution

The condition under which Eq. (14) satisfies the inequality constraints can be obtained by expanding Eq. (5) as a Taylor series

$$y(t) = A\left[1 - \cos\left(\frac{\pi t}{T}\right)\right]$$

$$= \frac{A}{2}\left(\frac{\pi t}{T}\right)^2 - \frac{A}{24}\left(\frac{\pi t}{T}\right)^4 + \cdots \tag{16}$$

If we combine Eqs. (5), (14), and (16), $x(t) \leq y(t)$ becomes

$$3(2A - L)\left(\frac{t}{T}\right)^2 - 2(2A - L)\left(\frac{t}{T}\right)^3 \leq \frac{A\pi^2}{2}\left(\frac{t}{T}\right)^2 - \frac{A\pi^4}{24}\left(\frac{t}{T}\right)^4 + \cdots \tag{17}$$

For small t/T,

$$3(2A - L) \leq A\pi^2/2$$

which yields the condition

$$L \geq [2 - (\pi^2/6)]A \tag{18}$$

The symmetry of the optimal trajectory and inequality constraints guarantees that this is also the sufficient condition for Eq. (14) to satisfy the inequality constraint near the final time.

VI. Suboptimal Solution

A suboptimal solution to Eq. (4) that automatically satisfies the inequality constraints of Eq. (5) is

$$x_{\text{sub}}(t) = (A - L/2)[1 - \cos(\pi t/T)], \qquad 2A - L > 0 \tag{19}$$

which has control history

$$u_{\text{sub}} = (A - L/2)(\pi^2/T^2)\cos(\pi t/T) \tag{20}$$

and rms acceleration

$$\text{rms}(\ddot{x}_{\text{sub}}) = (\sqrt{2}/4)\pi^2[(2A - L)/T^2] \tag{21}$$

When Eqs. (15) and (21) are compared, it is clear that the suboptimal solution is only slightly inferior to the optimal

$$[\text{rms}(\ddot{x}_{\text{opt}})/\text{rms}(\ddot{x}_{\text{sub}})] = (4\sqrt{6}/\pi^2) \approx 0.9927 \tag{22}$$

A comparison of the optimal and suboptimal accelerations and trajectories when condition (18) holds is shown in Fig. 3. The optimal solution when condition (18) is invalid is a combination of a linear control law and wall following trajectories,

$$u_{\text{opt}_2}(t) = \begin{cases} (A\pi^2/T^2)\cos(\pi t/T), & 0 \le t \le t^* \\ \alpha - 2\alpha t/T, & t^* < t < T - t^* \\ (A\pi^2/T^2)\cos(\pi t/T), & T - t^* < t < T \end{cases} \tag{23}$$

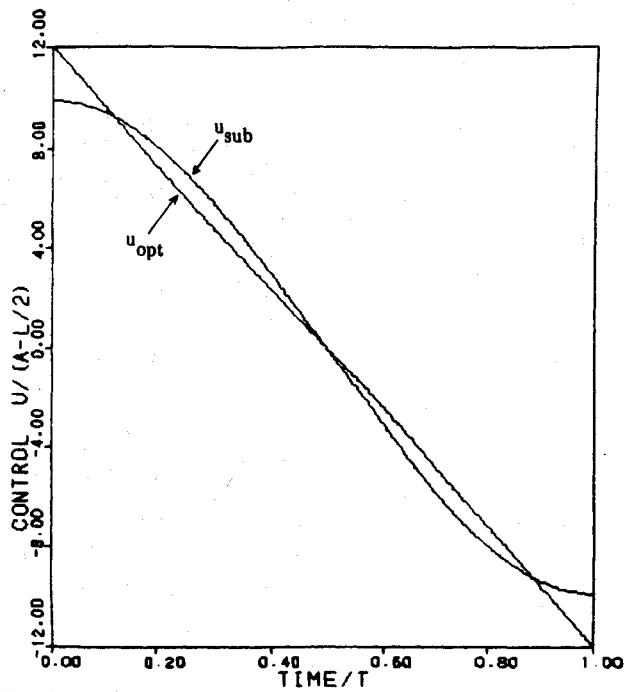

Fig. 3 Comparison of optimal and suboptimal acceleration histories.

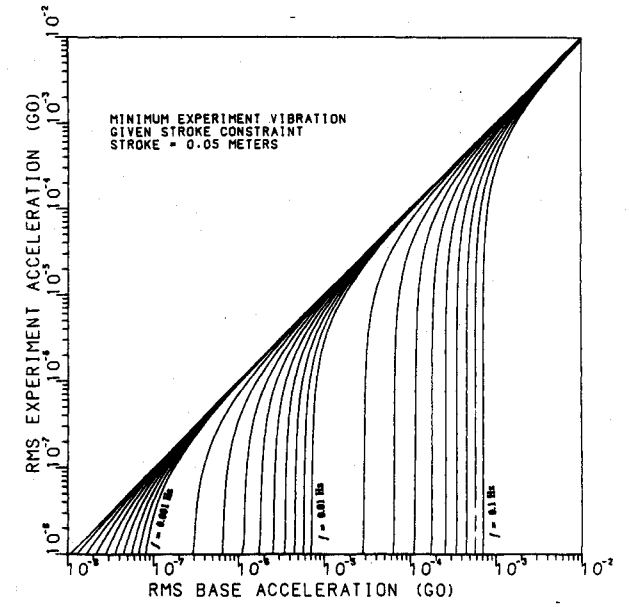

Fig. 4 Minimum experiment acceleration given disturbance frequency, stroke = 5 cm.

where t^* and α are determined by the solution of several transcendental equations expressing position and velocity continuity at t^*. It is clear that the rms of this optimal solution must be bounded between that of the suboptimal and the optimal with the inequality constraints of (5) dropped

$$(\sqrt{12})\frac{(2A - L)}{T^2} \le \text{rms}(u_{\text{opt}_2}) < \left(\frac{\sqrt{2}}{4}\pi^2\right)\frac{(2A - L)}{T^2}$$

$$3.4641\frac{(2A - L)}{T^2} < \text{rms}(u_{\text{opt}_2}) < 3.4895\frac{(2A - L)}{T^2} \tag{24}$$

The suboptimal solution can obviously be employed as an excellent approximation to the optimal, Eq. (23), when condition (18) is not satisfied.

VII. Limitations on Isolation

The primary purpose of this paper is to determine theoretical limits to vibration isolation. Although a dimensionless plot could have been produced, it was felt that a few typical dimensional plots would be of more use to designers of microgravity materials science experiments. Figures 4–6 present the curves of the minimum experiment acceleration vs base acceleration at constant frequencies for stroke limits of 5, 10, and 20 cm, respectively.

The horizontal axis gives the rms base acceleration calculated from

$$\text{rms}(\ddot{y}) = (\sqrt{2}/2)\omega^2 A \tag{25}$$

The vertical axis is the minimum experiment acceleration from Eq. (15) when Eq. (18) holds and Eq. (21) when it does not.

In Figs. 4–6, the minimum experiment rms acceleration at any given frequency is zero (isolation) until the base displacement amplitude equals one-half the maximum stroke possible. The minimum experiment rms then quickly rises with increases in base acceleration and asymptotically approaches the zero-vibration-reduction line, at 45 deg. Along this line, the base and experiment act as if they were rigidly coupled together and have the same acceleration.

The primary limitation is the length of stroke allowed between the experiment and the base. As an example calculation, consider an rms base acceleration of $1 \times 10^{-3}\, g_0$ at a frequency of 0.06 Hz. The base travel is given by

$$2A = 2\sqrt{2}[\text{rms}(\ddot{y})/\omega^2] \tag{26}$$

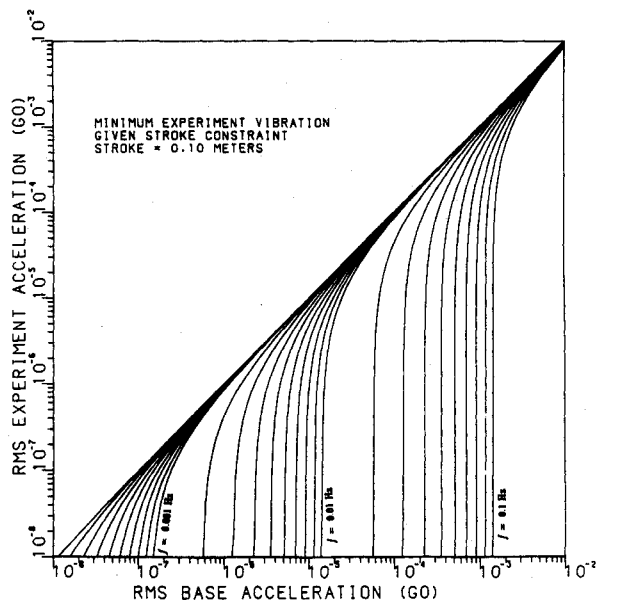

Fig. 5 Minimum experiment acceleration given disturbance frequency, stroke = 10 cm.

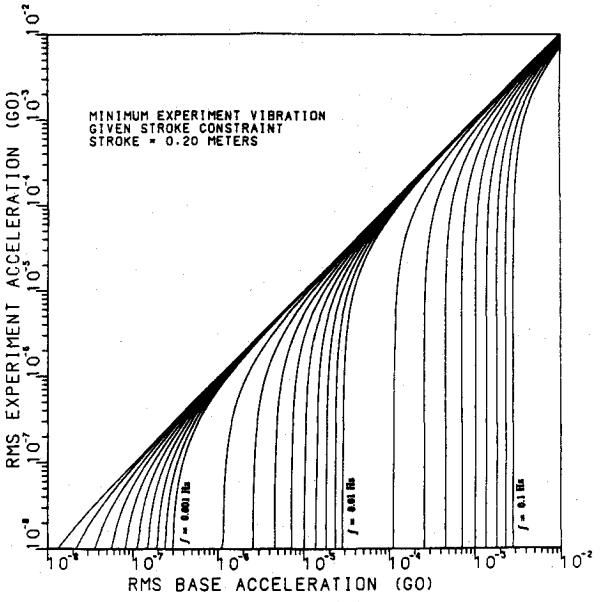

Fig. 6 Minimum experiment acceleration given disturbance frequency, stroke = 20 cm.

which has the numerical value of 19.5 cm for this example. For a stroke $L = 5$ cm, Fig. 4 shows that the experiment acceleration will be at least $7 \times 10^{-4}\, g_0$. When the stroke is increased to $L = 10$ cm, Fig. 5 gives a value of $4.5 \times 10^{-4}\, g_0$.

The last case is a stroke of $L = 20$ cm. Figure 6 indicates that the minimum acceleration is zero. In this case, $L > 2A$ so the stroke is large enough to accommodate the full sinusoidal motion without wall contact.

As an alternative to the plots, Eqs. (15), (18), (21), and (25) may be used directly. These can be simplified for this purpose to

$$\frac{\text{rms}(\ddot{x})}{\text{rms}(\ddot{y})} = \begin{cases} \left(1 - \dfrac{L}{2A}\right), & 0 \le \dfrac{L}{2A} < \left(1 - \dfrac{\pi^2}{12}\right) \\ \dfrac{4\sqrt{6}}{\pi^2}\left(1 - \dfrac{L}{2A}\right), & \left(1 - \dfrac{\pi^2}{12}\right) < \dfrac{L}{2A} < 1 \\ 0, & 1 < \dfrac{L}{2A} \end{cases} \quad (27)$$

with

$$2A = [2\sqrt{2}\,\text{rms}(\ddot{y})/\omega^2]$$

VIII. Conclusions

This paper has developed a kinematic formulation for the microgravity space experiment problem in one dimension. Further, two solutions, one optimal and the other suboptimal but very close to optimal, have been obtained. These permit plots of vibration attenuation for given levels of available space. For the sinusoidal oscillation assumed here, the experiment could be completely isolated if sufficient space were available. Unfortunately, the low-frequency motions (0–0.01 Hz) would require motions with a length much larger than possible aboard spacecraft.

Plots of the type developed here are intended to assist microgravity experiment designers as well as vibration isolation engineers. These plots represent the ideal vibration isolator. Real systems will not be able to attain the ideal for several reasons. The actual motion will have several frequency components as well as a random component. The random component alone will ensure that the full space L cannot be employed. Some safety space will have to be allocated to prevent occasional wall contact. Any real active control system will have some nonideal characteristics. The sensors employed in the active control feedback loop will have some errors as well. The authors of this paper are aware that the development of a very low-frequency accelerometer is difficult. In spite of this, we are optimistic about the levels of vibration isolation discussed here. It seems reasonable to believe that approximately 75% of ideal isolation is possible with an actual control system and actuator.

Acknowledgments

This work was supported, in part, by NASA Lewis Research Center and the Commonwealth of Virginia.

References

[1]Spencer, L., "Overview of NASA Microgravity Programs and Opportunities," Vibration Isolation Technology for Microgravity Science Workshop, NASA Lewis Research Center, Sept. 28–29, 1988.

[2]Alexander, J. I., "Experiment Sensitivity: Determination of Requirements for Isolation," Vibration Isolation Technology for Microgravity Science Workshop, NASA Lewis Research Center, Sept. 28–29, 1988.

[3]Sharpe, A. (ed.), "Low Acceleration Characterization of Space Station Environment," NASA Marshall Space Flight Center, Final Rept. SP85-MSFC-2928, Revision B, Oct. 1985.

[4]Stuhlinger, E., and Mookherji, T., "Materials Processing Twin Experiment," AIAA Paper 88-0348, Jan. 1988.

[5]Chassay, R. P., "Measurements by NASA," *Measurement and Characterization of the Acceleration Environment Onboard the Space Station*, Aug. 1986.

[6]Henderson, F., "MSL-2 Accelerometer Data Results," *Measurement and Characterization of the Acceleration Environment Onboard the Space Station*, Aug. 1986.

[7]Grodsinsky, C. M., and Brown, J. V., "Low Frequency Vibration Isolation Technology for Microgravity Space Experiments," 12th Biennial Conference on Mechanical Vibration and Noise, American Society of Mechanical Engineers, New York, NASA TM 101448, Sept. 1989.

[8]Fox, J. C., and McNally, P. J., "Current Orbiter Instrumentation and Acceleration Environment Data," Vibration Isolation Technology for Microgravity Science Workshop, NASA Lewis Research Center, Sept. 28–29, 1988.

[9]Hamacher, H., Jilig, R., and Merbold, U., "Analysis of Microgravity Experiments Performed During D1," Materials Science Under Microgravity Conditions, 6th European Symposium, Bordeaux, Dec. 2–5, 1986.

[10]Davis, L. P., Wilson, J. F., Jewell, R. E., and Roden, J. J., "Hubble Space Telescope Reaction Wheel Assembly Vibration Isolation System," March 1986.

[11]Wilson, J. F., and Davis, L. P., "Viscous Damped Space Structure for Reduced Jitter," 58th Shock and Vibration Symposium, Huntsville, AL, Aug. 1987.

[12]Hamilton, B. J., Andrus, J. H., and Carter, D. R., "Pointing Mount with Active Vibration Isolation for Large Payloads," 10th Annual Guidance and Control Conference, American Astronautical Society, Washington, DC, Jan.-Feb. 1987.

[13]Genkin, M. D., Yelezov, V. G., and Yablonsky, V. V., "Vibration Isolation System with Enhanced Effectiveness," *Vibration Engineering*, Vol. 2, 1988, pp. 183–186.

[14]Bryson, A. E., and Ho, Y.-C., *Applied Optimal Control: Optimization, Estimation, and Control*, Hemisphere, New York, 1975, pp. 108–127.

[15]Sage, A. P., and White, C. C., *Optimum Systems Control*, 2nd ed., Prentice-Hall, Englewood Cliffs, NJ, 1977, pp. 27–52.

[16]Elbert, T. F., *Estimation and Control of Systems*, Van Nostrand Reinhold, New York, 1989, pp. 262–346.

David H. Allen
Associate Editor